Non-intrusive Load Monitoring Based on Graph Total Variation for Residential Appliances

Xiaoyang Ma, Diwen Zheng, Xiaoyong Deng, Ying Wang, Dawei Deng, and Wei Li

***Abstract*—Non-intrusive load monitoring is a technique for monitoring the operating conditions of electrical appliances by collecting the aggregated electrical information at the household power inlet. Despite several studies on the mining of unique load characteristics, few studies have extensively considered the high computational burden and sample training. Based on low-frequency sampling data, a non-intrusive load monitoring algorithm utilizing the graph total variation (GTV) is proposed in this study. The algorithm can effectively depict the load state without the need for prior training. First, the combined *K*-means clustering algorithm and graph signals are used to build concise and accurate graph structures as load models. The GTV representing the internal structure of the graph signal is introduced as the optimization model and solved using the augmented Lagrangian iterative algorithm. The introduction of the difference operator decreases the computing cost and addresses the inaccurate reconstruction of the graph signal. With low-frequency sampling data, the algorithm only requires a little prior data and no training, thereby reducing the computing cost. Experiments conducted using the reference energy disaggregation dataset and almanac of minutely power dataset demonstrated the stable superiority of the algorithm and its low computational burden.**

***Index Terms*—Non-intrusive load monitoring, graph total variation, augmented Lagrangian function, smart grid.**

I. Introduction

With the gradual development of intelligent power consumption, power demand-side management technology, and energy conservation awareness, non-intrusive load monitoring (NILM) technology has attracted significant research attention. This technology identifies the operation status and energy consumption per appliance by obtaining total electrical information using specialized monitoring devices or smart meters. Previous research reveals that residential and commercial buildings account for a large part of the total energy consumption [1], which can be reduced by the appropriate adjustment of user electricity consumption plans [2]. The NILM is critical for the realization of a more refined demand-side response on the power supply side and the enhancement of customer electricity consumption patterns [3].

After the initial proposal of the NILM concept [4], a significant amount of research has been conducted on high-frequency sampling data to achieve load monitoring based on rich load features. Various studies [5] - [9] extract time-domain characteristics of signals such as active power and current harmonics to decompose the single signal from the total power consumption signal. The use of S-transform, wavelet transform, or other transformation methods to extract the frequency-domain characteristics can achieve the effective monitoring of the operation states of loads [10] - [12]. Establishing the *V-I* trajectory (mutual trajectory of the instantaneous voltage and steady-state current waveforms) of the load can improve the accuracy of load identification [13], [14]. The change in the appliance status results in a change in electrical quantities, which is reflected in the total power consumption information. With an increase in the number of unique load signatures, the identification and monitoring of appliances are enhanced. The novelty of this study on high-frequency sampling data is primarily related to the investigation of unique load signatures based on large amounts of priori electrical information. It should be noted that the aforementioned NILM algorithms have stringent requirements for data acquisition devices, which results in large data storage and processing costs, in addition to relatively low practicability.

Smart meters, which are extensively employed, are generally suitable at sampling rates with large intervals [15], due to the limitations of the manufacturing cost, storage cost, and data transmission capacity. The use of low-frequency sampling signals obtained by smart meters for data analysis and mining has become a new research hotspot [16], [17]. Considering that only steady-state features can be obtained during low-frequency sampling, the similarity of features between different electrical appliances leads to significant limitations.

To resolve the problem above, NILM algorithms based on low-frequency data can be roughly divided into two categories: based on event detection and based on state estimation.

Manuscript received: September 9, 2022; revised: March 16, 2023; accepted: October 7, 2023. Date of CrossCheck: October 7, 2023. Date of online publication: November 22, 2023.

This work was supported by National Natural Science Foundation of China (No. 52107117).

X. Ma and Y. Wang (corresponding author) are with the College of Electrical Engineering, Sichuan University, Chengdu 610065, China (e-mail: mxy_scu@163.com; tuantuan1125@scu.edu.cn).

D. Zheng and X. Deng are with State Grid Chongqing Electric Power Company, Chongqing 400014, China (e-mail: 864647962@qq. com; 895423929@qq. com).

D. Deng is with State Grid Sichuan Electric Power Company, Chengdu 610095, China (e-mail: 765572728@qq.com).

W. Li is with State Grid Hubei Electric Power Company Limited Research Institute, Wuhan 430077, China (e-mail: 820372462@qq.com).

DOI: 10.35833/MPCE.2022.000581

The event detection based algorithms identify changes in the load operation state by continuously detecting fluctuations in the total power signal. Commonly used algorithms include edge detection [18], neural networks [19], machine learning (ML) [20], support vector machines [21], and decision trees [22]. In [18], an adaptive detection threshold is introduced, which can be adjusted adaptively according to load fluctuation, to improve the capacity of detecting events with different amplitudes. In [19], a novel convolutional neural network (CNN) model with a recurrent property is proposed to more accurately capture energy signal interdependencies. Reference [20] presents a comprehensive performance evaluation model of 10 ML algorithms along with their comparative analysis. These algorithms introduced in the above research are influenced by the event detection results, which are directly related to the extent to which the operating characteristics of the appliance are accurately extracted. If one algorithm is highly sensitive to grid noise and cannot accurately determine the moment of the event, the accuracy of the algorithm is significantly reduced.

The state estimation based algorithms realize load monitoring by estimating the optimal combination of appliance time series. Hidden Markov models (HMMs) and their extensions are extensively used in such algorithms due to their capacity to determine the hidden state sequence from the observation sequence with the maximum probability [23]-[25]. An adaptive density peak clustering (ADPC) algorithm based on the factor hidden Markov model (FHMM) is proposed in [23], which reduces the dependence on prior information. Within the framework of the additive FHMM, an NILM algorithm based on the mixed active and reactive power features is proposed in [24], which maintains superior performance in noisy environments. In addition to the HMM-based algorithm, several algorithms are investigated to compensate for the lack of information in low-frequency sampling, and to mine new load features. Reference [26] uses the Karhunen-Loeve transform to enhance the difference between the steady-state characteristics of the active power and the maximum a posteriori estimation to complete load decomposition. Dynamic time warping (DTW) distance is widely used for pattern recognition between sequences due to its insensitivity to local amplitude differences and sequence lengths [27], [28]. In [27], the aggregate power signal is split into sub-series with single load operating or multiple load operating simultaneously, and the DTW distance is used as a similarity metric to determine the identification results. These state estimation algorithms are computationally complex and require a training step using sampling data in advance. In addition, the probability of reaching a local optimum when searching for the optimal combination is high.

Existing algorithms cannot balance accuracy and execution time when accurately building load models and extracting features. This paper introduces a graph structure as the data processing tool and proposes a novel NILM algorithm based on graph total variation (GTV), inspired by [29] and [30]. First, the combined *K*-means clustering algorithm and graph signals are used to build concise and accurate graph structures as load models. The total variation in the graph representing the internal structure of the graph signal is introduced as the optimization model and solved using the augmented Lagrangian iterative algorithm. The introduction of the difference operator decreases the computing cost and addresses the inaccurate reconstruction of the graph signal. With low-frequency sampling data, the algorithm requires a little prior data and no training, which reduces hardware and computing costs. As the test time increases, the performance and efficiency of the algorithm remain high; thus, the algorithm is suitable for long-term NILM. The proposed algorithm is tested using the reference energy disaggregation dataset (REDD) and the almanac of minutely power dataset (AMPds) to validate the superiority and low computational burden.

II. Theory

A. Problem Formulation of NILM

Different appliances generally reflect different electrical information during operation, such as active power, current, and harmonics. Different electrical information, also known as load characteristics, will be reflected in the total electrical signals. The core issue of NILM is how to identify the appliances' electrical signals through the load characteristics in the total electrical signal. For low-frequency sampling data, power signals are generally used for load monitoring. The relationship between the total power signal and the power signals of appliances can be expressed as:

$$\bar{x}_t = \sum_{l=1}^{L} x_t^l + n_t \tag{1}$$

where $\bar{x}_t$ is the total power value at moment t; L is the number of appliances; x_t^l is the power value of appliance l at moment t; and n_t is the error power caused by noise at moment t.

Therefore, the research task of NILM is to reconstruct the power values of household appliances at different moments for a given total power, so as to monitor the operation situation and energy usage of appliances. However, the load characteristics reflected in the power signal are too single, so graph signal is introduced to strengthen the correlation between the total power signal and the appliances' power signals, thereby improving the accuracy of reconstruction.

B. Basic Principles of Graph

Graphs, which are the basic objects of study in the graph theory, can represent the topology of real networks or abstractly represent the internal structure of datasets. The mathematical representation of a graph is $G(V,E)$, where $V=\{v_1, v_2, \ldots, v_n\}$ represents the set of vertices of the graph, and E represents the set of edges formed between vertices. The adjacency matrix $\boldsymbol{A}$ can reflect the internal relationship of a graph. It is composed of the weights of the edges of the graph structure, which is generally divided into unweighted and weighted adjacency matrices. The definition of the unweighted adjacency matrix is as follows. If two vertices in a graph are connected, the matrix element is 1; otherwise, the matrix element is 0. In general, the weighted adjacency ma-

trix is weighted in two manners: by the Euclidean distance and by the Gaussian kernel function. The Gaussian kernel function is the most commonly used kernel function in ML, which can appropriately reduce the difference between vertices. Hence, in this study, the Gaussian kernel function is employed to define the elements in the adjacency matrix:

$$A_{ij} = \exp(-\|x_i - x_j\|^2 / \rho^2) \tag{2}$$

where x_i and x_j are the values of the graph vertices i and j, respectively; and ρ is a scale parameter.

To ensure the numerical stability of the graph signal during the calculation, the adjacency matrix $\boldsymbol{A}$ is normalized as:

$$\boldsymbol{A}_{norm} = \frac{1}{|\lambda_{\max}|}\boldsymbol{A} \tag{3}$$

where $|\lambda_{\max}|$ is the maximum of the absolute values of the eigenvalues.

The reconstruction of the load profiles of household appliances requires discrete time signals, wherein only adjacent sample points are connected. Based on the structural characteristics, the load profile is constructed as a path graph, whose sampling points denote the vertices of the graph. If each vertex of the graph signal is assigned a value, the signal values of all vertices can form a vector $\boldsymbol{S}$ of graph signals, which is a dataset transformed from the graph structure that reflects the relationship between vertices in the graph. In the following expression, $\boldsymbol{S}$ can be defined as a column vector:

$$\boldsymbol{S} = [s_1 \quad s_2 \quad \ldots \quad s_n]^{\mathrm{T}} \quad s_i \in C \tag{4}$$

where C is the integer set; and each element $s_i \in \boldsymbol{S}$ represents the classification label of the graph vertex i. Based on the above, the graph signals of total power signal and appliances' power signals can be constructed.

C. GTV

The discrete derivative at the vertex i represents the graph variation of a single vertex, which can be calculated as:

$$\left.\frac{\mathrm{d}\boldsymbol{S}}{\mathrm{d}V}\right|_i = \nabla_i(\boldsymbol{S}) = s_i - \sum_{s_j \in \Re} A_{norm(i,j)} s_j \tag{5}$$

where $\Re = \{j | A_{ij} \neq 0\}$ is the set of vertices connected to vertex i. In discrete graph signal processing, GTV is often used to quantify the degree of change in the graph signal. The smaller the GTV, the smaller the fluctuation of the two vertex values connected by an edge. This parameter can be used as a judgment of the similarity between two graph signals, which converts the power feature into the graph characteristic. The GTV is calculated as:

$$TV_p = \left\| \boldsymbol{S} - \frac{1}{\lambda_{\max}(\boldsymbol{A})}\boldsymbol{A}\boldsymbol{S} \right\|_F^p \tag{6}$$

where $p = 1, 2, \ldots$; and $\|\cdot\|_F$ is the Frobenius norm.

The object of this paper is to use a graph signal with a non-fixed signal value. Thus, the total variation of the variable graph signal is calculated as:

$$TV_2 = \frac{1}{2}\left\| \boldsymbol{S} - \frac{1}{\lambda_{\max}(\boldsymbol{A})}\boldsymbol{A}\boldsymbol{S} \right\|_F^2 \tag{7}$$

The reconstruction of the graph signal can be expressed as the utilization of a certain amount of priori information (known data) to achieve the reconstruction of the unknown part. Due to the existence of noise in the time-varying signal, noise is taken into account in the reconstruction process. Equation (1) is expressed as the optimization function for minimizing the power error. To prevent overfitting, the cumulative function of the GTV is added as the regularization term, as shown in (8). Power signal reconstruction is converted into graph signal reconstruction problem.

$$\begin{aligned} F(\boldsymbol{S}) &= \arg\min_{\boldsymbol{S}} \|\boldsymbol{J} \circ \boldsymbol{S} - \boldsymbol{S}'\|_F^2 + \gamma \cdot TV_2(s) = \\ &\arg\min_{\boldsymbol{S}} \|\boldsymbol{J} \circ \boldsymbol{S} - \boldsymbol{S}'\|_F^2 + \frac{\gamma}{2}\left\| \boldsymbol{S} - \frac{1}{\lambda_{\max}(\boldsymbol{A})}\boldsymbol{A}\boldsymbol{S} \right\|_F^2 \end{aligned} \tag{8}$$

where $\boldsymbol{S}'$ is the graph signal containing prior information; γ is the normalized parameter; $\circ$ denotes the Hadamard product; and $\boldsymbol{J}$ is the diagonal matrix of prior information. If the i^{th} sampling point is known information, a value of 1 is assigned to the i^{th} diagonal element; otherwise, 0 is assigned. The first term of (8) is the kernel function of the calculation error, and the second term is the cumulative function of total variation. Then, the graph signal reconstruction problem can be transformed into an optimization problem to determine an appropriate $\boldsymbol{S}$ to minimize (8).

III. Methodology

This section details the development of the graph structure based on the total power consumption data obtained from the NILM device. According to (2), the adjacency matrix $\boldsymbol{A}$ is established, and x_i and x_j herein are the active power values at sampling points i and j, respectively.

A. Graph Signal of Discrete Power Signal

In a given household, suppose there are L electrical appliances with stable operating states. The power consumption signal of appliance l contains n sampling points, where the first q points are known ($(x_1^l, x_2^l, \ldots, x_q^l)$ are the priori power consumption data of appliance l) and the final $n-q$ points are unknown. To construct the simplified graph signal with priori information, the combined K-means clustering algorithm is adopted to convert power values into graph label values. First, K is initialized to $\sqrt{q}$. After classical K-means clustering, the overlap rate of the circles with a maximum cluster radius corresponding to different cluster centers is used to determine whether similar clusters are merged. When two clusters are merged, update the structure of the merged clusters. Repeat this process until all clusters do not satisfy the merge conditions.

The calculation equation of the distance between an element in cluster a and the central element in cluster b is expressed as:

$$d_{atb} = \left| x_{at} - c_b \right| \tag{9}$$

where x_{at} is the t^{th} element of cluster a; and c_b is the central element of cluster b.

Define the maximum radius of cluster b as:

$$r_b = \max(|x_{bt} - c_b|) \tag{10}$$

where x_{bt} is the t^{th} element of cluster b.

The overlap parameter ε is initially set to be 0. When the distance d_{atb} does not exceed the maximum radius r_b, 1 is added to the overlap parameter ε; otherwise, the value remains the same. When all the Q_a elements in cluster a are compared, the ratio $\delta=\varepsilon/Q_a$ is calculated. If the ratio is greater than the threshold, clusters a and b are combined into a new cluster; otherwise, they remain distinct clusters. The threshold value is set to be 0.8 in this study. Thereafter, the algorithm outputs different clusters with the corresponding maximum and minimum values, taking the appropriate values to construct the threshold vector $\boldsymbol{M}$. The value closest to the cluster center is selected as the threshold. If the cluster center is at the same distance from the maximum and minimum values, the value of the cluster center is selected as the threshold.

$$\boldsymbol{M}=\begin{bmatrix} m_1 & m_2 & \dots & m_\vartheta \end{bmatrix} \tag{11}$$

where ϑ is the number of clusters output by the algorithm; and m_ϑ is the ϑ^{th} power threshold obtained based on the combined K-means clustering algorithm.

The graph signal of the known priori information of appliance l can be expressed as:

$$s_i^l=\begin{cases} \vartheta & x_i^l > m_\vartheta \\ \vartheta-1 & m_{\vartheta-1} < x_i^l \le m_\vartheta \\ \vdots & \\ 1 & m_1 < x_i^l \le m_2 \\ 0 & 0 < x_i^l \le m_1 \end{cases} \tag{12}$$

where s_i^l is the graph signal value of appliance l at moment i ($i=1,2,\dots,q$); and x_i^l is the active power of appliance l at moment i. The unknown $n-q$ graph signal values are set to be 0. Thus, the priori graph signal of appliance l can be written as $\boldsymbol{S}'^{l}=[s_1^l, s_2^l, \dots, s_q^l, 0, 0, \dots, 0]^{\mathrm{T}}$. The unknown graph signal of an appliance can be solved using the adjacency matrix $\boldsymbol{A}$ constructed from the total sampling data and (8).

B. Augmented Lagrangian Iterative Algorithm for Solving Graph Signal

Before reconstructing the graph signal of the device, the difference method is used to improve the smoothness of the data to achieve good performance. The mathematical definition of the difference operator $\boldsymbol{D}$ can be expressed as:

$$\boldsymbol{D}=\begin{bmatrix} \boldsymbol{Z} & \boldsymbol{0} \\ \boldsymbol{0} & \boldsymbol{B} \end{bmatrix} \tag{13}$$

$$\boldsymbol{Z}=\begin{bmatrix} -1 & 0 & \dots & 0 \\ 1 & 0 & \dots & 0 \\ \vdots & \vdots & & \vdots \\ 0 & 0 & \dots & -1 \\ 0 & 0 & \dots & 1 \end{bmatrix}_{q\times q} \tag{14}$$

$$\boldsymbol{B}=\begin{bmatrix} 1 & 0 & \dots & 0 \\ 0 & 1 & \dots & 0 \\ \vdots & \vdots & & \vdots \\ 0 & 0 & \dots & 1 \end{bmatrix}_{(n-q)\times(n-q)} \tag{15}$$

Therefore, the graph signal $\boldsymbol{S}'$ in (8) is expressed as $\boldsymbol{S}''=\boldsymbol{D}\boldsymbol{S}'=[s_2-s_1, s_3-s_2, \dots, s_q-s_{q-1}, 0, 0, \dots, 0]^{\mathrm{T}}$. The reconstruction problem of the time-varying graph signal expressed by (8) includes two main components: the error minimization problem and the cumulative function of the GTV. They are both convex functions, which can be solved using the alternating direction method of multipliers (ADMM). By introducing the similarity matrix $\tilde{\boldsymbol{S}}$ of the graph signal matrix $\boldsymbol{S}$, (8) is transformed into:

$$\begin{cases} F(\boldsymbol{S})=\arg\min\limits_{\boldsymbol{S}} \left\| \boldsymbol{J}\circ\boldsymbol{S}-\boldsymbol{S}'' \right\|_F^2+\dfrac{\gamma}{2}\left\| \boldsymbol{S}-\dfrac{1}{\lambda_{\max}(\boldsymbol{A})}\boldsymbol{A}\boldsymbol{S} \right\|_F^2 \\ \text{s.t. } \boldsymbol{S}=\tilde{\boldsymbol{S}} \end{cases} \tag{16}$$

The augmented Lagrangian iterative algorithm is introduced to solve the problem because of its simple principle, easy implementation, and good performance in convex optimization problems. The augmented Lagrangian function of (16) is expressed as:

$$L(\boldsymbol{S},\tilde{\boldsymbol{S}},\boldsymbol{\mu},\tau)=\frac{\gamma}{2}\left\| \tilde{\boldsymbol{S}}-\frac{1}{\lambda_{\max}(\boldsymbol{A})}\boldsymbol{A}\tilde{\boldsymbol{S}} \right\|_F^2+\left\langle \boldsymbol{\mu},\boldsymbol{S}-\tilde{\boldsymbol{S}} \right\rangle+\tau\left\| \boldsymbol{S}-\tilde{\boldsymbol{S}} \right\|_F^2 \tag{17}$$

where $\boldsymbol{\mu}$ is the Lagrange multiplier; τ is the regularization parameter; and $\langle\cdot\rangle$ denotes the inner product of the matrix. The iterative solution formulas are calculated as:

$$\boldsymbol{S}^{k+1}=\arg\min_{\boldsymbol{S}} L(\boldsymbol{S}^k,\tilde{\boldsymbol{S}}^k,\boldsymbol{\mu}^k,\tau)=\arg\min_{\boldsymbol{S}}\left\| \boldsymbol{J}\circ\boldsymbol{S}-\boldsymbol{S}'' \right\|_F^2+\left\langle \boldsymbol{\mu}^k,\boldsymbol{S}-\boldsymbol{S}^k \right\rangle+\tau\left\| \boldsymbol{S}^k-\tilde{\boldsymbol{S}}^k \right\|_F^2 \tag{18}$$

$$\tilde{\boldsymbol{S}}^{k+1}=\arg\min_{\tilde{\boldsymbol{S}}} L(\boldsymbol{S}^k,\gamma,\boldsymbol{\mu}^k,\tau)=\arg\min_{\tilde{\boldsymbol{S}}}\frac{\gamma}{2}\left\| \tilde{\boldsymbol{S}}^k-\frac{1}{\lambda_{\max}(\boldsymbol{A})}\boldsymbol{A}\tilde{\boldsymbol{S}}^k \right\|_F^2+\left\langle \boldsymbol{\mu}^k,\boldsymbol{S}-\tilde{\boldsymbol{S}}^k \right\rangle+\tau\left\| \tilde{\boldsymbol{S}}^k-\boldsymbol{S}^k \right\|_F^2 \tag{19}$$

$$\boldsymbol{\mu}^{k+1}=\boldsymbol{\mu}^k+\tau(\boldsymbol{S}^{k+1}-\tilde{\boldsymbol{S}}^{k+1}) \tag{20}$$

where k is the iterative number.

The singular contraction operator is used to minimize calculation errors. If each $\tau>0$ and $\boldsymbol{Y}\in\mathbf{R}^{n\times 1}$, the singular value shrinkage operator obeys:

$$S_\tau(\boldsymbol{Y})=\min_{\boldsymbol{Z}}\left(\frac{1}{2}\left\| \boldsymbol{Z}-\boldsymbol{Y} \right\|_F^2\right)+\tau\left\| \boldsymbol{Z} \right\|_* \tag{21}$$

where $\boldsymbol{Y}=\boldsymbol{J}\circ\boldsymbol{S}-\boldsymbol{S}''$; and $\|\cdot\|_*$ denotes the nuclear norm. For the operator $S_\tau(\boldsymbol{Y})$, suppose the singular value decomposition (SVD) of a matrix $\boldsymbol{Y}=\boldsymbol{U}\boldsymbol{\Sigma}\boldsymbol{V}^{\mathrm{T}}$, where $\boldsymbol{U}$ and $\boldsymbol{V}$ are the orthogonal matrices, and $\boldsymbol{\Sigma}$ is the diagonal matrix. Then, the shrinkage operator is defined as:

$$f_\tau(\boldsymbol{S})=\boldsymbol{U}\mathrm{diag}(s_\tau(\sigma_{\boldsymbol{\Sigma}}))\boldsymbol{V}^{\mathrm{T}} \tag{22}$$

where $\sigma_{\boldsymbol{\Sigma}}$ denotes the singular values of matrix $\boldsymbol{\Sigma}$; and $s_\tau(\sigma_{\boldsymbol{\Sigma}})=\max(\sigma_{\boldsymbol{\Sigma}}-\tau,0)$. When the constraint condition $\partial\tilde{\boldsymbol{S}}^{k+1}/\partial\tilde{\boldsymbol{S}}=\boldsymbol{0}$ is satisfied, the global optimal solution is obtained.

$$\tilde{\boldsymbol{S}}^{k+1}=(2\gamma\mathrm{diag}(\boldsymbol{J})+\tau\boldsymbol{I})^{-1}(2\gamma\boldsymbol{A}+\boldsymbol{\mu}^k+\tau\boldsymbol{S}^k) \tag{23}$$

where $\boldsymbol{I}$ is the identity matrix.

The steps for solving the unknown graph signal using the augmented Lagrangian iterative algorithm can be summarized as follows.

Step 1: initialize the input parameters such as adjacency matrix $\boldsymbol{A}$, regularization parameter ρ, normalization parameter γ, the maximum number of iterations K, and iteration abort threshold ξ.

Step 2: initialize the iteration parameter $k=1$, the graph signal matrix $\tilde{\boldsymbol{S}}^1=\boldsymbol{S}''$, and the Lagrangian coefficient $\boldsymbol{\mu}^1=\boldsymbol{S}''$.

Step 3: obtain the updated matrix $\boldsymbol{S}^{k+1}=f_\tau(\tilde{\boldsymbol{S}}^k-\boldsymbol{\mu}^k/\tau)$ by solving (22).

Step 4: solve $\tilde{\boldsymbol{S}}^{k+1}$ based on (23), and update $\boldsymbol{\mu}^{k+1}$ based on (20).

Step 5: if $k\geq K$ and $\|\boldsymbol{S}^{k+1}-\tilde{\boldsymbol{S}}^{k+1}\|\leq\xi$, the iterative process is completed, and the reconstructed graph signal $\boldsymbol{S}$ is obtained. Otherwise, let $k=k+1$, and return to *Step 3*.

C. Load Profile Reconstruction Based on Graph Signal

Based on (11) and (12), the graph signal value reflects the change in state of the appliance. If the signal value is 0, the state of the device does not change. If the signal value is not 0, this reflects a change in the active power of the appliance; thus, the switching time of the appliance can be monitored. Therefore, the operating duration of the appliance can be derived from the number of sampling points between a non-zero graph signal value and an adjacent non-zero graph signal value.

The graph signal $\boldsymbol{S}$, as mentioned in Section III-B, is the dataset after applying the differential operation, which cannot be directly utilized to reconstruct the load profile of appliances. The differential inverse operation of $\boldsymbol{S}$ is then carried out as:

$$\boldsymbol{S}^*=\boldsymbol{Z}_{n\times n}^{-1}\boldsymbol{S} \tag{24}$$

Relating the elements in $\boldsymbol{S}^*$ to (12), the time-varying signal of the appliance can be obtained. When the load profile of one appliance is reconstructed, it is removed from the total power signal to reduce the interference from other appliances. Thereafter, the adjacency matrix of the new total power signal and priori graph signal of the following appliance are established. NILM is completed when the active power curves of all appliances are reconstructed.

In summary, the flowchart for NILM based on the GTV is shown in Fig. 1, and specific steps are presented below.

Step 1: the total power consumption data are obtained by sampling at the outlet of the power line, and the graph adjacency matrix is constructed based on (2) and (3). The prior power consumption information of appliances in the house is collected in advance.

Step 2: the combined K-means clustering algorithm is used to cluster the prior information of the load curve of the target equipment, and the threshold vector is established based on (11). Moreover, based on (12), the prior graph signal of the target appliance is established. Different graph signal values reflect different operating states of the equipment.

Step 3: by using the augmented Lagrangian iterative algorithm, the unconstrained optimization function, namely (8), is solved iteratively, and the reconstructed graph signal of the unknown part of the target appliance is obtained.

Step 4: based on the sampling points between a non-zero graph signal value and an adjacent non-zero graph signal value, the duration of a certain stable operating state of an appliance can be confirmed. The graph signal is restored to the power consumption signal, and the load profile reconstruction of the target appliance is completed.

Step 5: the active power signal is removed, and a new adjacency matrix of the new total power signal and priori graph signal of the following appliance are established. NILM is completed when the active power curves of all appliances are reconstructed.

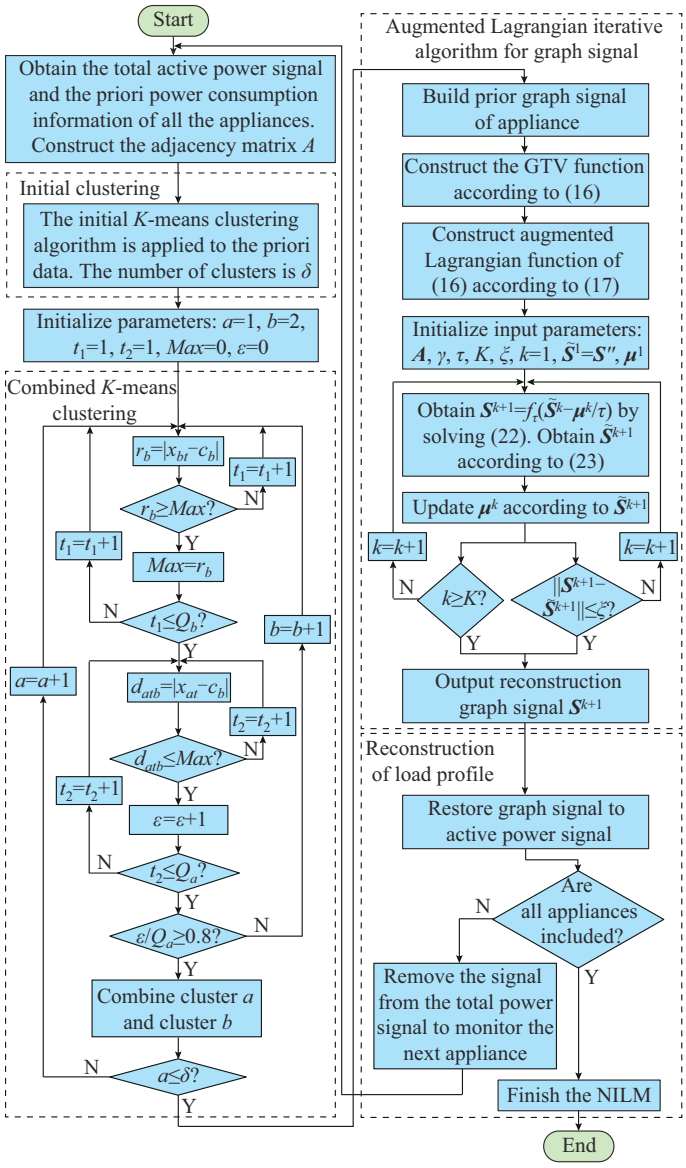

Fig. 1. Flowchart for NILM based on GTV.

IV. Results and Discussion

A. Dataset and Test Sample

In this subsection, the REDD [31] containing the data of residential consumption in the United States and the AMPds developed in [32] are employed to validate the proposed algorithm. The REDD contains the power consumption data of six houses, in which the low-frequency dataset is logged at a frequency of approximately once a second for the mains and

once every three seconds for the circuits. The AMPds contains the energy data of one house in Canada within a year, and the sampling frequency is 1/60 Hz. Due to the high sparsity of appliance power signals at the time-scale, it is difficult to strictly meet the integrity of power consumption information in a short period of time. The power signals of appliances for three consecutive days with a sampling interval of 1 min are used as the experimental sample. The power signal from Day 1 is used to construct the priori graph signal, and the power signals from the following two days are aggregated as the total power signal to evaluate and verify the proposed algorithm.

B. Evaluation Metrics

To comprehensively evaluate the performance of load profile consumption, five commonly used evaluation metrics are employed in this study.

In particular, the aforementioned metrics for evaluating the performance of power signal reconstruction are *Accuracy*, *Precision*, *Recall*, and F1-measure F_{M}, which are defined as:

$$Accuracy = \frac{TP + TN}{TP + TN + FP + FN} \tag{25}$$

$$Precision = \frac{TP}{TP + FP} \tag{26}$$

$$Recall = \frac{TP}{TP + FN} \tag{27}$$

$$F_{\mathrm{M}} = \frac{2 \cdot Precision \cdot Recall}{Precision + Precision} \tag{28}$$

The four possible outcomes from a binary classifier are defined as follows [33]: *TP* denotes the number of times an appliance is accurately detected as on; *TN* denotes the number of times an appliance is accurately detected as off; *FP* denotes the number of times an appliance is inaccurately detected as on; and *FN* denotes the number of times an appliance is inaccurately detected as off. Moreover, F_{M} is the harmonic mean of *Precision* and *Recall*.

The metric used to evaluate the proportion of total power correctly assigned *PTCA* [31] is expressed as:

$$PTCA = 1 - \frac{\sum_{t=1}^{T}\sum_{i=1}^{m}\left| p_t^{(i)} - \hat{p}_t^{(i)} \right|}{2\sum_{t=1}^{T}\bar{p}_t} \tag{29}$$

where $p_t^{(i)}$ and $\hat{p}_t^{(i)}$ are the real and calculated active power of appliance i at time t, respectively; and $\bar{p}_t$ is the aggregated power measured during sample time t.

C. Test Scenarios and Results

1) Scenario 1: AMPds (7 Appliances)

This scenario involves 7 appliances: clothes dryer (CDE), clothes washer (CWE), kitchen fridge (FGE), dishwasher (DWE), heat pump (HPE), wall oven (WOE), in addition to an entertainment system consisting of a television (TV), personal video recorder (PVR), and AMP, which is denoted as TVE. The results obtained by applying the proposed algorithm to Scenario 1 are shown in Fig. 2.

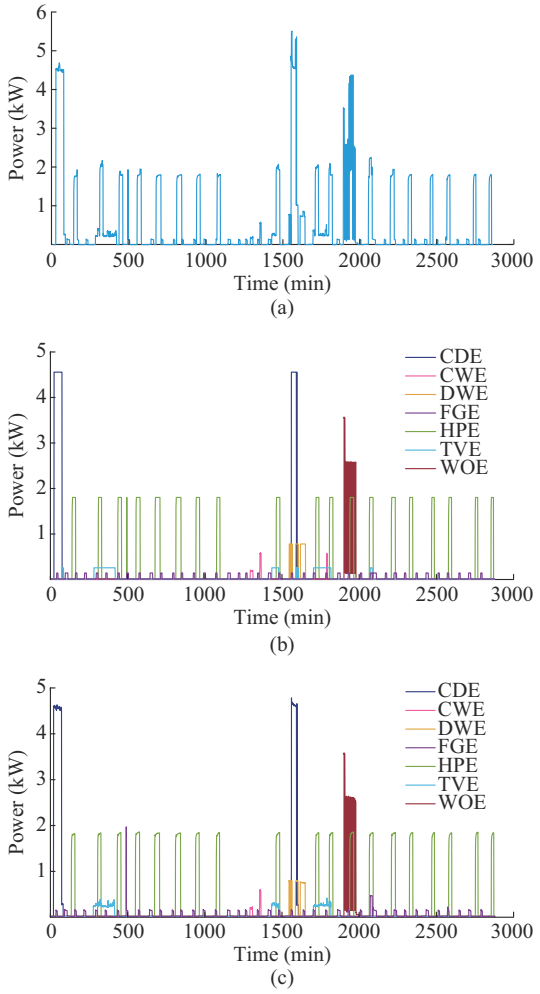

Fig. 2. Results of Scenario 1 over a time period of 48 hours. (a) Total power. (b) Estimated disaggregated power consumption via proposed algorithm. (c) True disaggregated power consumption.

As can be observed from a comparison between Fig. 2(b) and (c), the proposed algorithm accurately identifies the states of most appliances, including the correct on/off time and the corresponding power values, thus indicating the feasibility and effectiveness of the proposed algorithm. When the power of two devices is highly similar or the combined power is similar, the algorithm is prone to misjudge. For example, the CDE with the low power gear is inaccurately detected as TVE at approximately 70 min, and the FGE with the higher transient power is inaccurately detected as HPE at 490 min. Besides, when FGE operates simultaneously with CDE in high power gear or WOE, the low-power features of FGE will be overwritten by other high-power features, thus resulting in more false negative events. To quantify the recognition performance of each appliance more accurately, the *Accuracy* and F_{M} metrics of GTV are calculated, as shown in Table I.

Based on the results, each appliance exhibits a relatively high *Accuracy* of 0.95 or a higher value. The CDE and WOE exhibit a *Precision* score of 1, with low *Recall* scores due to the inaccurate detection of low-power states. Besides, the *Recall* of WOE is higher, which may be due to the fre-

quent switching between two states during operation. The GTV is sufficiently large to accurately identify characteristics in iterative reconstruction. This indicates that the reconstruction effect of the proposed algorithm is not influenced by abrupt power changes. The TVE gains the lowest *Precision* score, as it is frequently detected as a false positive event.

TABLE I
Accuracy, *Precision*, *Recall*, AND F_M OF PROPOSED ALGORITHM IN SCENARIO 1

Appliance	*Accuracy*	*Precision*	*Recall*	F_M
CDE	0.9658	1.0000	0.7963	0.8866
CWE	0.9897	0.9333	0.9655	0.9491
DWE	0.9894	0.9347	0.9581	0.9463
FGE	0.9726	0.9351	0.9057	0.9202
HPE	0.9813	0.9580	0.9716	0.9647
TVE	0.9514	0.8611	0.9254	0.8921
WOE	0.9686	1.0000	0.8851	0.9390
Average	0.9741	0.9460	0.9153	0.9283

Estimating power consumption is a critical part of load monitoring and the basis of power saving. A pie chart calculating the percentage of power consumed by each appliance during the test time is shown in Fig. 3.

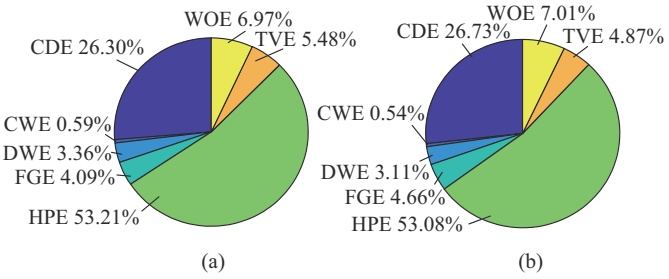

Fig. 3. Pie chart of power consumption of each appliance in Scenario 1. (a) Estimated power consumption. (b) True power consumption.

It can be observed from Fig. 3 that the CDE and HPE consume most energy. This is because the CDE power is the highest and the working duration is not short; whereas, the HPE exhibits a lower power, and is used frequently. Besides, as can be observed from Fig. 3, the energy assignments by the proposed algorithm are very close to the ground truth, whereas FGE and TVE exhibit relatively high errors. This can be attributed to their inaccurate detection, and their F_M scores are lower. It should be noted that these two metrics are not completely correlated, given that the F_M score of the CDE is low. However, the energy error is not high. Given that false negative events only occur in low power gear operations, the proportion of the true power consumption is significantly small with respect to the total power consumption.

To further verify the performance of the proposed algorithm, a comparison is made with the HMM [25], sparse representation-based classification (SRC) [34], and CNN [35] algorithms. The average values of the aforementioned evaluation metrics and the *PTCA* are calculated, as shown in Table II.

TABLE II
COMPARISON OF PROPOSED, HMM, SRC, AND CNN ALGORITHMS IN SCENARIO 1

Algorithm	*Accuracy*	*Precision*	*Recall*	F_M	*PTCA*
GTV	0.9741	0.9460	0.9153	0.9283	0.9075
HMM	0.9585	0.9148	0.8775	0.8958	0.8955
SRC	0.9611	0.9347	0.9167	0.9251	0.8824
CNN	0.9515	0.8858	0.8936	0.8897	0.8669

The *Accuracy* metric exhibits a value greater than 0.95, given that most appliances are mainly in the OFF state. However, *Accuracy* is a common evaluation metric that is unsuitable for the evaluation of NILM algorithms. The proposed algorithm demonstrates higher performance than the other algorithms with respect to the average scores of the five metrics, which indicates the superiority of the proposed algorithm. The *Recall* score is slightly lower than that of the SRC algorithm. This is because the main advantage of the SRC algorithm is its capacity to infer from little priori data. On occasion, the proposed algorithm exhibits an inaccurate detection of states when there is a little prior data. The *PTCA* exceeds the other algorithms and reaches a value of 0.9075 due to the introduction of a differential inverse operation in the conversion process between the graph signal and the power signal, thus resulting in a small reconstruction error.

2) Scenario 2: REDD (11 Appliances in House 3)

In this scenario, 11 appliances such as a microwave and lighting in House 3 are selected for simulation analysis of the proposed algorithm with the load monitoring results, as shown in Fig. 4.

As can be observed from a comparison between Figs. 2 and 4, the operating conditions in Scenario 2 are more complex; thus, the inaccurate detection of the appliance status is more frequent. The appliance category with the highest detection error is electronics. In particular, it is inaccurately detected as dishwasher or refrigerator, and is not detected when using washer_dryer1. The power of the refrigerator is low with significantly high transient power on occasion when switched on, thus leading to inaccurate detection. The proposed algorithm exhibits a preference toward the detection of simple scenarios instead of those involving complex combinations. For example, the simultaneous usage of washer_dryer1 and refrigerator is detected as washer_dryer2. The evaluation metrics obtained based on the calculation results are shown in Table III.

As shown in Table III, the detection of lighting1 yields the highest F_M scores. This can be mainly attributed to the unique power value and independent operating period. Electronics exhibits significantly low *Accuracy* and F_M scores. This is because the low power gear is detected as a high power gear, resulting in numerous false positive and false negative events. In particular, two modes are mismatched, thus generating numerous false positive and false negative events simultaneously. The dishwasher gains the lowest *Recall* score, because one of the modes is inaccurately detected as electronics. When its true positive events are few, the in-

crease in false negative events significantly reduces the *Recall* score. The microwave gains a low *Recall* score for the same reason. Moreover, washer_dryer1 is inaccurately detected as washer_dryer2. Thus, the former has more false negative events and a low *Recall* score; whereas, the latter has more false positive events and a low *Precision* score.

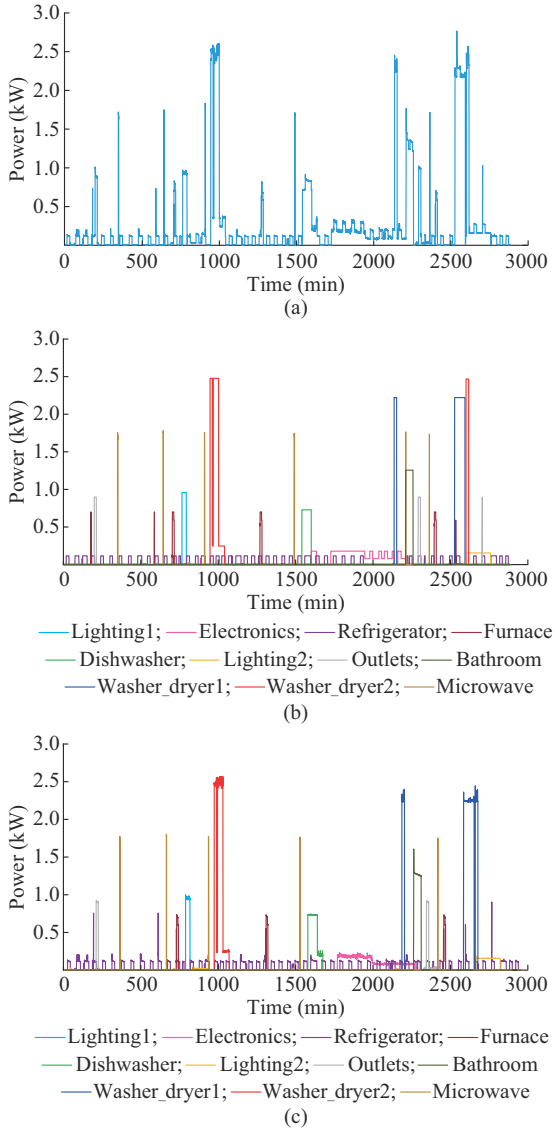

Fig. 4. Results of Scenario 2 over a time-period of 48 hours. (a) Total power. (b) Estimated disaggregated power consumption via proposed algorithm. (c) True disaggregated power consumption.

The power consumption ratio of each appliance is calculated within the test time, as shown in Fig. 5. To improve the clarity of the pie chart, the first four letters of each appliance are displayed in addition to the relevant number. The error fluctuations for this scenario are not significantly larger than those for Scenario 1. Washer_dryer1 and washer_dryer2 consume most of the power. However, the power consumption error is large due to the mismatch between the two appliances. Electronics exhibits a large power consumption error due to an excessive number of inaccurate detections. The detection errors related to the other electrical appliances with small power consumptions such as lighting, outlets, and microwave are not significant. Overall, as can be observed from Fig. 5, the energy assignments by the proposed algorithm are relatively close to the ground truth, where most of the difference is exhibited by washer_dryer1 (with energy assignment of 22.15% instead of 16.69%) and washer_dryer2 (with energy assignment of 23.34% instead of 27.66%). The results validate the effectiveness and efficiency of the proposed algorithm with respect to monitoring power consumption.

TABLE III
Accuracy, *Precision*, *Recall*, AND F_M OF PROPOSED ALGORITHM IN SCENARIO 2

Appliance	*Accuracy*	*Precision*	*Recall*	F_M
Lighting1	0.9796	1.0000	0.9655	0.9824
Electronics	0.9071	0.5833	0.6512	0.6154
Refrigerator	0.9422	0.9375	0.9000	0.9184
Dishwasher	0.9578	0.9677	0.6452	0.7747
Furnace	0.9779	0.9070	0.9512	0.9286
Lighting2	0.9658	0.8611	0.9254	0.8921
Outlets	0.9789	0.8750	0.9333	0.9032
Washer_dryer1	0.9731	0.9545	0.8400	0.8936
Washer_dryer2	0.9624	0.8559	0.9406	0.8963
Microwave	0.9797	0.8333	1.0000	0.9091
Bathroom	0.9786	0.9600	0.9796	0.9697
Average	0.9639	0.8850	0.8847	0.8803

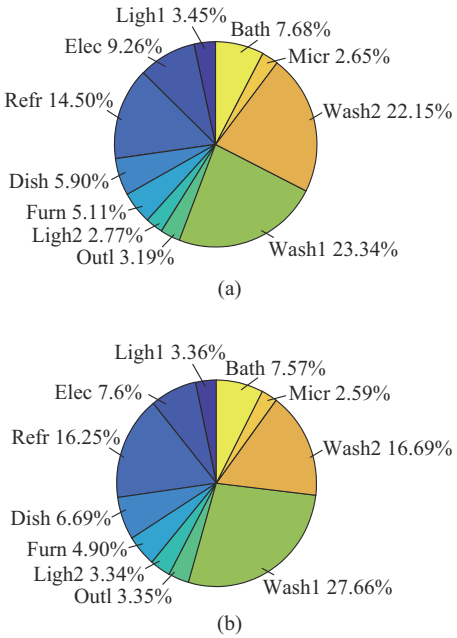

Fig. 5. Pie chart of power consumption per appliance in Scenario 2. (a) Estimated power consumption. (b) True power consumption.

A comparison between the proposed algorithm and the other three algorithms is shown in Table IV.

When the number of appliances is increased to 11, the performance of the proposed algorithm decreases compared with Scenario 1; however, it exhibits a superior performance among all algorithms. This can be mainly attributed to the differential operation on the graph signal, which improves

the smoothing characteristics of the data. In the function of the GTV, the reconstructed graph signal is closer to the real value. The HMM algorithm is most negatively influenced by the increase in the number of appliances, and the evaluation metric scores are the lowest. The increase in the sequence length of the HMM algorithm may lead to an exponential increase in the algorithm complexity, which influences the accuracy of the algorithm. The SRC algorithm exhibits more inaccurate detection cases in this scenario than the proposed algorithm, and the proportion of incorrectly assigned energy is greater, thus exhibiting a lower *PTCA* score. The application of the proposed algorithm outperforms all other algorithms with respect to the evaluation metrics among all samples.

TABLE IV
COMPARISON OF PROPOSED, HMM, SRC, AND CNN ALGORITHMS IN SCENARIO 2

Algorithm	*Accuracy*	*Precision*	*Recall*	F_M	*PTCA*
GTV	0.9639	0.8850	0.8847	0.8849	0.8521
HMM	0.9287	0.8295	0.7839	0.8061	0.7884
SRC	0.9615	0.8687	0.8426	0.8555	0.8317
CNN	0.9470	0.8472	0.8498	0.8485	0.8269

3) Scenario 3: Influence of Sampling Interval Setting

As can be observed from the first two scenarios, the performance of algorithms decreases with the increase in the number of appliances. The degree of reduction is related to the specific operating conditions of each appliance within a day. In addition, this scenario is investigated to test the influence of the sampling frequency on the results of the proposed algorithm and the compared algorithms. The data from the two aforementioned scenarios are down-sampled to 2 min per sampling point for testing, and the calculation results for *PTCA* scores are depicted as a histogram in Fig. 6.

When calculating the *PTCA* score, one sampling point is still recorded per minute, and the calculated power value of the un-sampled point is equal to the reconstructed power value of the previous minute. If the *PTCA* score calculated according to the power value of 2 min misses the error between the real and estimated values of the un-sampled points, it may have a higher score than before, which has no reference significance. As can be observed from the histogram, in the same scenario, all algorithms exhibit a decrease in the *PTCA* score when the sampling frequency is reduced and the algorithm performances are negatively influenced. This is because the general operating cycle of electrical appliances ranges from a few minutes to several minutes, which leads to the filtering of numerous details of the source signal, thus resulting in an incapacity to approximately fit the source signal. In contrast, the proposed algorithm outperforms all other algorithms regardless of the size or variation of the *PTCA* score. The results obtained using the HMM algorithm are the same as those described above. The *PTCA* score abruptly decreases due to an increase in the number of appliances, and it is not significantly influenced by the sampling interval. Although the SRC algorithm is significantly influenced by the sampling interval, the down-sampling results for both scenarios exhibit the lowest scores. In particular, the CNN algorithm is less influenced by the number of appliances and sampling frequency, which demonstrates a relatively high robustness. However, the decomposition performance is not satisfactory. The test results indicate that the proposed algorithm can maintain high performance with a larger number of appliances and larger sampling intervals.

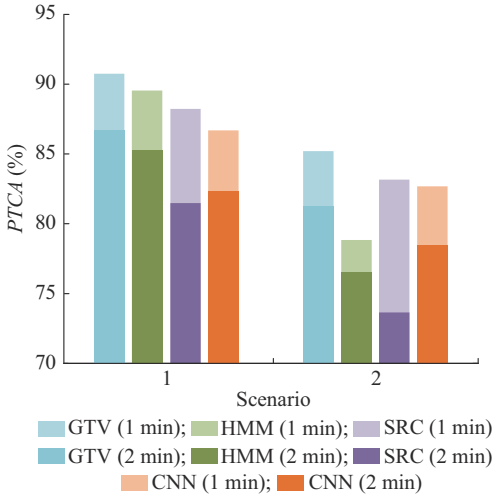

Fig. 6. Histogram of *PTCA* scores with respect to different sampling frequencies and scenarios.

In practice, considering the data collected at a higher sampling frequency as a priori information significantly improves the accuracy. However, the high sampling frequency poses stringent requirements for power data sampling equipment, and significantly increases the computation cost of data. Meanwhile, due to the high sparsity of electrical signals, as the sampling frequency increases, the corresponding sparsity matrix becomes larger, which significantly increases the solution difficulty and solution error. Hence, 1 min is selected as the sampling frequency in this study.

4) Computational Performance

In order to verify the superiority of the proposed algorithm without additional training, the total execution time of the comparison algorithms is recorded. As shown in Table V, the time required to build the load model and testing (per day) for each algorithm (t_L and t_T) in Scenarios 1 and 2 is included.

TABLE V
EXECUTION TIME OF PROPOSED, HMM, SRC, AND CNN ALGORITHMS IN SCENARIOS 1 AND 2

Scenario	Proposed		HMM		SRC		CNN	
	t_L (s)	t_T (s)	t_L (s)	t_T (s)	t_L (s)	t_T (s)	t_L (s)	t_T (s)
1	5.6	15.7	18.1	15.4	12.4	18.9	13.9	22.9
2	10.2	41.4	63.6	57.3	21.5	60.3	25.6	60.2

It can be observed from Table V that the proposed algorithm has the best performance, regardless of the time spent in processing the prior load data or in testing. In terms of horizontal comparison, the load data pre-processing time of the proposed algorithm is shorter than that of the other algo-

rithms, which indicates the advantage of the proposed algorithm without training in advance. The time cost of testing using the proposed algorithm is lower than that of the SRC and CNN algorithms, and it is only higher than that of the HMM algorithm in Scenario 1. However, the HMM algorithm consumes an excessive amount of time in load training, resulting in a significant increase in its total execution time, and its overall computational efficiency is not high. In the two scenarios, the proposed algorithm exhibits the highest computational efficiency. In the longitudinal comparison, when the number of appliances increases, t_L of the HMM algorithm increases rapidly while that of the other algorithms increases slowly. Once a new appliance is added to the scenario or the scenario is changed, such algorithms need to adjust or even rebuild the load model, which can be time-consuming. The time consumed for the testing of all algorithms increases approximately exponentially. This confirms the exponential complexity of the scalability of the NILM problem. The proposed algorithm builds priori load models, which require some computational cost but consume much less time compared to the other algorithms, to train the load models. An accurate description of the load model is the basis of load monitoring. The proposed algorithm is also efficient in the test part, and it can be effectively applied to long-term NILM. In general, the proposed algorithm has advantages in computational performance and efficiency.

5) Impact of Test Time on Algorithm Performance

In order to further verify the performance and stability of the proposed algorithm, the number of test days (the original test time is 2 days, supplementing the experimental results of the first day) is increased to 10 days based on the data in Scenarios 1 and 2. Figure 7 shows the variation in the *PTCA* score and total execution time (the sum of the time spent on building load model and testing) with different test time.

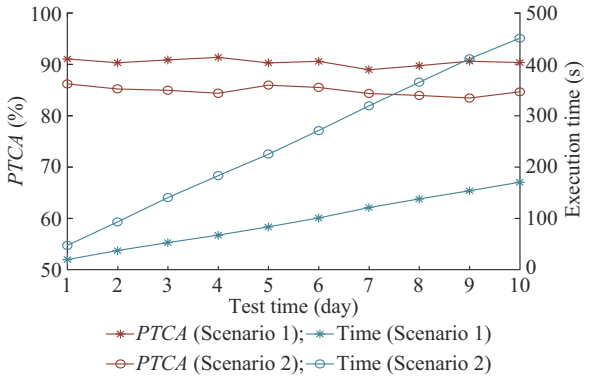

Fig. 7. Variation in *PTCA* score and total execution time with different test time.

The red lines indicate that the *PTCA* scores of the two scenarios fluctuate within the test time but do not significantly decrease as the test time increases. The proposed algorithm shows similar performance results on different test data. The generation of fluctuations is related to the complexity of the data and the number of input appliances, which is in line with the actual power consumption situation and reflects the stable performance of the proposed algorithm. The blue lines indicate that the total execution time of the two scenarios increases steadily during the test time, without a sharp increase. This means that the time consumed by the proposed algorithm to process each day's test data is stable. The proposed algorithm divides the test time into a time window of 1440 sampling points per day for multiple calculations. The length includes the complete cycle of the appliances' operation but does not cause a sharp increase in the execution time due to the large number of sampling points. Therefore, when the test time increases, the execution time of the proposed algorithm increases steadily. In general, the proposed algorithm has stable performance and can be effectively applied to the long-term NILM.

V. Conclusion

In this paper, a novel NILM algorithm based on the GTV is proposed to tackle the existing difficulties in mining load features of power signals and the limitation of accuracy and computational efficiency. In this paper, the power signal is converted into graph signal, and the applications of the adjacency matrix and GTV in the field of NILM are deeply explored. The main advantage of the proposed algorithm is to effectively depict the load state without the need for prior training. Based on low-frequency sampling data, the proposed algorithm can accurately and efficiently monitor the power signal and electricity consumption of appliances. Experiments conducted using the REDD and AMPds demonstrated the effectiveness and superior performance of the proposed algorithm, which has a good application prospect in the field of smart meters.

It should be noted there are several limitations to this study. The proposed algorithm cannot monitor appliances with complex operating modes and new states that are not in prior data. Mining the load features of complex appliances and the transition relationship between states are within the scope of future research. In addition, smart meters are gradually applied to non-intrusive technology. Adapting the algorithm to be reasonably compatible with smart meters is also to be carried out in the future.

References

[1] L. Pérez-Lombard, J. Ortiz, and C. Pout, "A review on buildings energy consumption information," *Energy and Buildings*, vol. 40, no. 3, pp. 394-398, Jan. 2008.
[2] J. Froehlich, E. Larson, S. Gupta *et al*., "Disaggregated end-use energy sensing for the smart grid," *IEEE Pervasive Computing*, vol. 10, no. 1, pp. 28-39, Jan. 2011.
[3] S. Makonin, L. G. Flores, R. Gill *et al*., "A consumer bill of rights for energy conservation," in *Proceedings of 2014 IEEE Canada International Humanitarian Technology Conference*, Montreal, Canada, Jun. 2014, pp. 1-6.
[4] G. W. Hart, "Nonintrusive appliance load monitoring," *Proceedings of the IEEE*, vol. 80, no. 12, pp. 1870-1891, Dec. 1992.
[5] M. Dong, P. C. M. Meira, W. Xu *et al*., "Non-intrusive signature extraction for major residential loads," *IEEE Transactions on Smart Grid*, vol. 4, no. 3, pp. 1421-1430, Sept. 2013.
[6] J. Liang, S. K. K. Ng, G. Kendall *et al*., "Load signature study – part I: basic concept, structure, and methodology," *IEEE Transactions on Power Delivery*, vol. 25, no. 2, pp. 551-560, Apr. 2010.
[7] S. Houidi, F. Auger, H. Sethom *et al*., "A review on buildings energy consumption information," *Energy and Buildings*, vol. 208, no. 109624, pp. 1-14, Feb. 2020.
[8] S. Ghosh, A. Chatterjee, and D. Chatterjee, "An improved load feature

extraction technique for smart homes using fuzzy-based NILM," *IEEE Transactions on Instrumentation and Measurement*, vol. 70, pp. 1-9, Jul. 2021.
[9] Y. Himeur, A. Alsalemi, F. Bensaali *et al*., "Effective non-intrusive load monitoring of buildings based on a novel multi-descriptor fusion with dimensionality reduction," *Applied Energy*, vol. 279, p. 115872, Dec. 2020.
[10] P. Held, S. Mauch, A. Saleh *et al*., "Frequency invariant transformation of periodic signals (FIT-PS) for classification in NILM," *IEEE Transactions on Smart Grid*, vol. 10, no. 5, pp. 5556-5563, Sept. 2019.
[11] J. Chen, X. Wang, X. Zhang *et al*., "Temporal and spectral feature learning with two-stream convolutional neural networks for appliance recognition in NILM," *IEEE Transactions on Smart Grid*, vol. 13, no. 1, pp. 762-772, Jan. 2022.
[12] C. Mariño, E. Masquil, F. Marchesoni *et al*., "NILM: multivariate DNN performance analysis with high frequency features," in *Proceedings of 2021 IEEE PES Innovative Smart Grid Technologies Conference – Latin America* (*ISGT Latin America*), Lima, Peru, Sept. 2021, pp. 1-5.
[13] Y. Liu, X. Wang, and W. You, "Non-intrusive load monitoring by voltage-current trajectory enabled transfer learning," *IEEE Transactions on Smart Grid*, vol. 10, no. 5, pp. 5609-5619, Sept. 2019.
[14] Z. Zhou, Y. Xiang, H. Xu *et al*., "Unsupervised learning for non-intrusive load monitoring in smart grid based on spiking deep neural network," *Journal of Modern Power Systems and Clean Energy*, vol. 10, no. 3, pp. 606-616, May 2022.
[15] M. Z. A. Bhotto, S. Makonin, and I. V. Bajić, "Load disaggregation based on aided linear integer programming," *IEEE Transactions on Circuits and Systems II*: *Express Briefs*, vol. 64, no. 7, pp. 792-796, Jul. 2017.
[16] G. Bucci, F. Ciancetta, E. Fiorucci *et al*., "State of art overview of non-intrusive load monitoring applications in smart grids," *Measurement*: *Sensors*, vol. 18, p. 100145, Dec. 2021.
[17] L. Morales-Velazquez, R. de J. Romero-Troncoso, G. Herrera-Ruiz *et al*., "Smart sensor network for power quality monitoring in electrical installations," *Measurement*, vol. 103, pp. 133-142, Jun. 2017.
[18] W. Luan, Z. Liu, B. Liu *et al*., "An adaptive two-stage load event detection method for nonintrusive load monitoring," *IEEE Transactions on Instrumentation and Measurement*, vol. 71, pp. 1-14, Dec. 2022.
[19] M. Kaselimi, E. Protopapadakis, A. Voulodimos *et al*., "Multi-channel recurrent convolutional neural networks for energy disaggregation," *IEEE Access*, vol. 7, pp. 81047-81056, Jun. 2019.
[20] A. U. Rehman, T. T. Lie, B. Vallès *et al*., "Comparative evaluation of machine learning models and input feature space for non-intrusive load monitoring," *Journal of Modern Power Systems and Clean Energy*, vol. 9, no. 5, pp. 1161-1171, Sept. 2021.
[21] P. Franco, J. M. Martínez, Y. C. Kim *et al*., "IoT based approach for load monitoring and activity recognition in smart homes," *IEEE Access*, vol. 9, pp. 45325-45339, Mar. 2021.
[22] T. T. H. Le, H. Kang, and H. Kim, "Household appliance classification using lower odd-numbered harmonics and the bagging decision tree," *IEEE Access*, vol. 8, pp. 55937-55952, Mar. 2020.
[23] Z. Wu, C. Wang, W. Peng *et al*., "Non-intrusive load monitoring using factorial hidden Markov model based on adaptive density peak clustering," *Energy and Buildings*, vol. 244, p. 111025, Aug. 2021.
[24] R. Bonfigli, E. Principi, M. Fagiani *et al*., "Non-intrusive load monitoring by using active and reactive power in additive factorial hidden Markov models," *Applied Energy*, vol. 208, pp. 1590-1607, Dec. 2017.
[25] T. Ji, L. Liu, T. Wang *et al*., "Non-intrusive load monitoring using additive factorial approximate maximum a posteriori based on iterative fuzzy *C*-means," *IEEE Transactions on Smart Grid*, vol. 10, no. 6, pp. 6667-6677, Nov. 2019.
[26] C. Dinesh, B. W. Nettasinghe, R. I. Godaliyadda *et al*., "Residential appliance identification based on spectral information of low frequency smart meter measurements," *IEEE Transactions on Smart Grid*, vol. 7, no. 6, pp. 2781-2792, Nov. 2016.
[27] A. Cominola, M. Giuliani, D. Piga *et al*., "A hybrid signature-based iterative disaggregation algorithm for non-intrusive load monitoring," *Applied Energy*, vol. 185, pp. 331-344, Jan. 2017.
[28] A. Iwayemi and C. Zhou, "SARAA: semi-supervised learning for automated residential appliance annotation," *IEEE Transactions on Smart Grid*, vol. 8, no. 2, pp. 779-786, Mar. 2017.
[29] A. Sandryhaila and J. M. F. Moura, "Discrete signal processing on graphs: frequency analysis," *IEEE Transactions on Signal Processing*, vol. 62, no. 12, pp. 3042-3054, Jun. 2014.
[30] K. He, L. Stankovic, J. Liao *et al*., "Non-intrusive load disaggregation using graph signal processing," *IEEE Transactions on Smart Grid*, vol. 9, no. 3, pp. 1739-1747, May 2018.
[31] J. Z. Kolter and M. J. Johnson, "REDD: a public data set for energy disaggregation research," *Artificial Intelligence*, vol. 25, pp. 1-6, Jan. 2011.
[32] S. Makonin, F. Popowich, L. Bartram *et al*., "AMPds: a public dataset for load disaggregation and eco-feedback research," in *Proceedings of 2013 IEEE Electrical Power & Energy Conference*, Halifax, Canada, Aug. 2013, pp. 1-6.
[33] R. Machlev, J. Belikov, Y. Beck *et al*., "MO-NILM: a multi-objective evolutionary algorithm for NILM classification," *Energy and Buildings*, vol. 199, pp. 134-144, Sept. 2019.
[34] S. Singh and A. Majumdar, "Non-intrusive load monitoring via multi-label sparse representation-based classification," *IEEE Transactions on Smart Grid*, vol. 11, no. 2, pp. 1799-1801, Mar. 2020.
[35] H. Rafiq, X. Shi, H. Zhang *et al*., "Generalizability improvement of deep learning-based non-intrusive load monitoring system using data augmentation," *IEEE Transactions on Smart Grid*, vol. 12, no. 4, pp. 3265-3277, Jul. 2021.

Xiaoyang Ma received the B.S., M.S., and Ph.D. degrees in electrical engineering from Sichuan University, Chengdu, China, in 2011, 2014, and 2018, respectively. He is currently an Associate Researcher with the College of Electrical Engineering, Sichuan University. His research interests include power quality analysis and renewable energy.

Diwen Zheng received the B.S. and M.S. degrees in electrical engineering from Sichuan University, Chengdu, China, in 2020 and 2023, respectively. She is presently working in State Grid Chongqing Electric Power Company, Chongqing, China. Her research interests include demand side management and non-intrusive monitoring.

Xiaoyong Deng received the B.S. degree in power system and automation from Wuhan University of Hydraulic and Electric Engineering, Wuhan, China, in 1999. Then, he received the M.S. degree from Chongqing Technology and Business University, Chongqing, China, in 2013. He is presently working in State Grid Chongqing Electric Power Company, Chongqing, China. His research interests include power system control and management.

Ying Wang received the B.S., M.S., and Ph.D. degrees in 2004, 2007, and 2014, respectively, from Sichuan University, Chengdu, China. During her Ph.D. study, she was a Visiting Student in electric power engineering with the Luleå University of Technology, Skellefteå, Sweden. Currently, she is an Associate Professor with Sichuan University. Her main research interests are in the area of voltage sags.

Dawei Deng received the B.S. degree in power system and automation from Xihua University, Chengdu, China, in 2008. He is presently working in State Grid Sichuan Electric Power Company, Chengdu, China. His research interests include high voltage power testing and maintenance.

Wei Li received the M.S. degree in hydropower and information engineering from Huazhong University of Science and Technology, Wuhan, China, in 2009. He is presently working in State Grid Hubei Electric Power Company Limited Research Institute, Wuhan, China. His current research interests include power quality analysis and voltage sags control.